29th Congress of the International Council of the Aeronautical Sciences
St. Petersburg, Russia; September 7-12, 2014

MACH NUMBER EFFECT ON THE FLOWFIELD STRUCTURE OF HYPERSONIC GAP FLOWS

Luis T. L. C. Paolicchi and Wilson F. N. Santos
Combustion and Propulsion Laboratory (LCP)
National Institute for Space Research (INPE)
Cachoeira Paulista, SP, 12630-000 Brazil

Keywords: *DSMC, Rarefied flow, Hypersonic flow, Gap, Compressibility effect*

Abstract

This paper presents the results of a numerical study of hypersonic gap flow in the transition flow regime by using the Direct Simulation Monte Carlo (DSMC) method. The sensitivity and characteristics of the flowfield structure are examined by varying the freestream Mach number and the gap length-to-depth (L/H) ratio. The proposed work focuses on the effect of the primary properties, velocity, density, pressure and temperature, due to variations in these two properities, i.e., freestream Mach number of 5, 15 and 25, and gap L/H ratio of 1, 1/2, 1/3, and 1/4. Some significant differences in the gap flow topology were noted between transition flow regime and continuum flow regime. For the conditions investigated, it was found only one vortex core inside the gaps instead of a column of vortices usually observed inside the gaps in the continuum flow regime. The analysis showed that the primary properties behavior inside the gaps for Mach number of 5 differed markedly from those for Mach number of 15 and 25. Conversely, the behavior of the properties for Mach number of 15 is similar to that for Mach number of 25.

1 Introduction

The study of fluid flow separation has been an important area of fluid mechanics research for decades. A separated flow may be produced by either imposing a pressure rise on an established boundary layer or by terminating the surface on which the boundary layer has developed. The former is observed by deflecting a control surface, while the latter occurs at the base of bodies and at the upstream edge of cavities and gaps. Such flows are of considerable interest to flight vehicle designers. Usually, they are associated with problems of control effectiveness, base drag, and base heating of missiles. In addition, the separated flow over a cavity or gap is of interest in those cases where recesses are to be found in the aerodynamic surface of flight vehicles.

The presence of gaps in modern aerodynamics configurations occurs as a desired or undesired design feature. For instance, the thermal protection systems of vehicles like the Space Shuttle orbiter require gaps between the used protection elements in order to accommodate thermal expansion and deflection of the primary structure. This protection is usually designed as an assembly of tiles. Tile arrays are oriented to minimize the ingress of hot boundary-layer gases into the tile gaps. The gaps between the tiles may modify the boundary layer state and eventually promote transition, inducing higher temperature levels than expected.

In regard to aerodynamic characteristics of gap flow, research studies [1, 2, 3, 4, 5, 6, 7, 8, 9, 10, 11] have been conducted in order to evaluate heating effects by considering the turbulent heating measurements related to the thermal damage on the Space Shuttle, even though much of the reentry trajectory provides laminar edge conditions on the vehicle. However, the majority of these research studies found in the current litera-

ture has gone into considering laminar or turbulent flow over a wide range of Mach numbers in the continuum flow regime. Nevertheless, there is little understanding of the physical aspects of hypersonic flow past to gaps in the transition flow regime, i.e., between free collision flow regime and continuum flow regime, associated to a reentry vehicle.

In this fashion, Paolicchi and Santos [12] have studied gaps situated in a rarefied hypersonic flow by employing the DSMC method. The work was motivated by the interest in investigating the effects of the gap L/H ratio on the aerodynamic surface quantities. The analysis showed that the aerodynamic quantities acting on the gap surface depended on the L/H ratio, for the range of conditions investigated. It was found that pressure and heat loads presented peak values at the corner of the gap forward face. Results showed that these loads were much larger than those attained in a smooth surface, represented by a flat plate without a gap.

In continuation of the gap study, the present account extends further the previous analysis [12] by investigating the impact of the compressibility on the flowfield structure. In this way, the primary goal of this paper is to assess the sensitivity of the primary properties, such as velocity, density, pressure, and temperature, due to variations on the freestream Mach number for a family of gaps defined by different L/H ratio. The focus of the present study is the low-density region in the upper atmosphere. In such a circumstance, the DSMC method will be employed to calculate the hypersonic two-dimensional flow over the gaps.

2 Geometry Definition

The gap geometry is the same as that presented by Paolicchi and Santos [12]. It was assumed a flat plate with a gap of length L and depth H. Figure 1 illustrates a schematic view of the model employed. The flat plate was selected by considering that the gap depth H is much smaller than the nose radius R of a reentry vehicle, i.e., $H/R \ll 1$. Therefore, the hypersonic flow over the flat plate with a gap may be representative of the hypersonic flow over a gap located on the surface of a reentry vehicle.

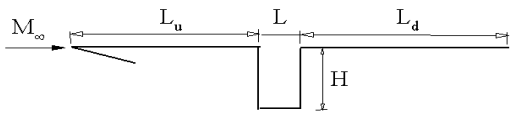

Fig. 1 Drawing illustrating a schematic view of the gap configuration.

According to Fig. 1, M_∞ stands for the freestream Mach number, H is the gap depth, L is the gap length, L_u the length of the gap upstream surface, and L_d the length of the gap downstream surface. It was assumed a length L of 3 mm, and a depth H of 3, 6, 9, and 12 mm. Therefore, the gaps investigated correspond to a length-to-depth ratio, L/H, of 1, 1/2, 1/3 and 1/4, respectively. In addition, L_u/λ_∞ of 50 and L_d/λ_∞ of 50, where λ_∞ is the freestream mean free path. It was considered that the flat plate is infinitely long but only the total length $L_u + L + L_d$ is investigated.

3 Freestream and Flow conditions

Freestream flow conditions used in the present simulations are those given by Paolicchi and Santos [12], and summarized in Tab. 1. These flow conditions represent those experienced by a capsule at an altitude of 70 km. This altitude is associated with the transitional flow regime, which is characterized by the overall Knudsen number the order of or larger than 10^{-2}.

Simulations are performed using a non-reacting gas model consisting of two chemical species, N_2 and O_2. Gas properties [13] are tabulated in Tab. 2, where χ, m, d and ω account respectively for mole fraction, molecular mass, molecular diameter, and viscosity index for O_2 and N_2.

The freestream velocity U_∞, assumed to be constant at 1486, 4456, and 7546 m/s, corresponds to a freestream Mach number M_∞ of 5, 15, and 25, respectively. The translational and vibrational temperatures in the freestream are in equilibrium at 219.07 K, and the gap surface has

Table 1 Freestream flow conditions.

Parameter	Value	Unit
Velocity (U_∞	1486/4456/7546	m/s
Temperature (T_∞)	219.07	K
Pressure (p_∞)	5.518	N/m^2
Density (ρ_∞)	8.752×10^{-5}	kg/m^3
Viscosity (μ_∞)	1.6280×10^{-5}	Ns/m^2
Number density (n_∞)	1.8193×10^{21}	m^{-3}
Mean free path (λ_∞)	9.285×10^{-4}	m

Table 2 Gas properties.

	χ	m (kg)	d (m)	ω
O_2	0.237	5.312×10^{-26}	4.01×10^{-10}	0.77
N_2	0.763	4.650×10^{-26}	4.11×10^{-10}	0.74

a constant wall temperature T_w of 880 K for all cases considered.

The overall Knudsen number Kn is defined as the ratio of the molecular mean free path λ in the gas to a characteristic dimension of the flowfield. By assuming the gap depth H as the characteristic length, the Knudsen number Kn_∞ corresponds to 0.3095, 0.1548, 0.1032, and 0.0774 for depth H of 3, 6, 9, and 12 mm, respectively. Finally, the Reynolds number Re_∞, based on the gap depth H and on conditions in the undisturbed stream, is in the range from 27 to 487 for the L/H ratio investigated.

4 Computational Tool

Flow in the regime of intermediate Knudsen numbers, $0.01 < Kn < 10$, is difficult to deal with analytically and, nowadays, it appears that the Direct Simulation Monte Carlo (DSMC) method, introduced by Bird [13], is the most accurate and credible procedure for computing thermal non-equilibrium effects in this flow regime. It is based on kinetic gas theory and does not depend on the continuum assumption that is not valid for high Knudsen number gas flows.

DSMC method models the flow as being a large number of statistically representative molecules, each one with a position, velocity and internal energy. Based on the assumptions of dilute gas and molecular chaos, the DSMC method only considers binary collisions. The molecular motion and their collisions are uncoupled when the computational time step is smaller than the physical collision time. At the beginning of the simulation, the simulated molecules are uniformly distributed statistically in the cells. At each step, all molecules move according to their individual velocities. As the simulated molecules move, they may collide with other simulated molecules or interact with the physical boundaries. In this process, both momentum and energy are conserved. After fulfilling all the required molecular movements, the collisions between particles are simulated in each cell independently. These steps are repeated until the statistical scatters are small enough. Finally, the macroscopic characteristics of the flow are obtained by sampling the molecular properties in each cell.

In the present study, the molecular collisions are modeled by using the variable hard sphere (VHS) molecular model [14], and the no time counter (NTC) collision sampling technique [15]. The VHS model employs the simple hard sphere angular scattering law so that all directions are equally possible for post-collision velocity in the center-of-mass frame of reference. However, the collision cross section depends on the relative speed of colliding molecules.

Energy exchange between kinetic and internal modes is controlled by the Borgnakke-Larsen statistical model [16]. The essential feature of this model is that part of collisions is treated as completely inelastic, and the remainder of the molecular collisions is regarded as elastic. Energy exchanges between the translational and internal modes of the two chemical species, N_2 and O_2, are considered. The probability of an inelastic collision determines the rate at which energy is transferred between the translational and internal modes after an inelastic collision. For a given collision, the probabilities are designated by the inverse of the relaxation numbers, which corre-

spond to the number of collisions necessary, on average, for a molecule to relax. Relaxation collision numbers are obtained in a collision energy-based procedure as suggested by Boyd [17] for rotation and by Bird [18] for vibration.

5 Computational Flow Domain and Grid

In order to implement the collision process, the flowfield around the gap is divided into an arbitrary number of regions, which are subdivided into computational cells. The cells are further subdivided into subcells, two subcells/cell in each coordinate direction. In this way, the cell provides a convenient reference for the sampling of the macroscopic gas properties, while the collision partners are selected from the same subcell for the establishment of the collision rate. The dimensions of the cells must be such that the change in flow properties across each cell is small. The linear dimensions of the cells should be small in comparison with the scale length of the macroscopic flow gradients normal to streamwise directions, which means that the cell dimensions should be the order of or even smaller than the local mean free path [13].

The computational domain used for the simulation is made large enough so that body disturbances do not reach the upstream and side boundaries, where freestream conditions are specified. A schematic view of the computational domain is illustrated in Fig. 2. Based on this figure, the computational domain was divided into five regions. In addition, side I-A is defined by the gap surface. Diffuse reflection with complete thermal accommodation is the condition applied to this side. Side I-B is a plane of symmetry, where all flow gradients normal to the plane are zero. At the molecular level, this plane is equivalent to a specular reflecting boundary. Sides II and III are the freestream sides through which simulated molecules enter and exit. Side II is positioned at $5\lambda_\infty$ upstream of the flat-plate leading edge, and side III defined at $30\lambda_\infty$ above the flat plate. Finally, the flow at the downstream outflow boundary, side IV, is predominantly supersonic and vacuum condition is specified [13]. At this boundary, simulated molecules can only exit. It is important to remark that, close to the wall, molecules may not be moving at supersonic speed. As a result, in this subsonic region close to the wall, there is an interaction between the flow and the downstream boundary. Nevertheless, the extent of the upstream effect of this boundary condition can be determined by changing the length of surface S5. In doing so, it was found [19] that the upstream disturbance is approximately of $6\lambda_\infty$.

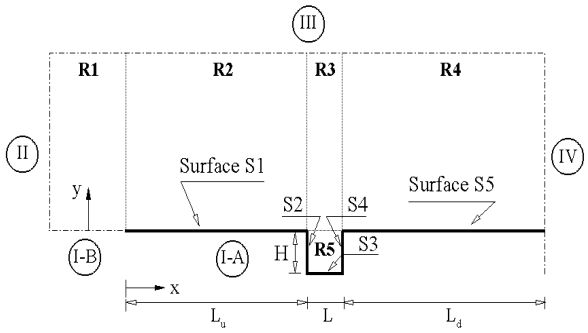

Fig. 2 Drawing illustrating a schematic view of the computational domain.

The numerical accuracy in the DSMC method depends on the computational cell size and on the number of particles per computational cell. Both effects were investigated to determine the number of cells and the number of particles required to achieve grid independence solutions for the thermal non-equilibrium flow over the gaps. A grid independence study was made with three different structured meshes – coarse, standard and fine – in each coordinate direction. The effect of altering the cell size in the x–direction was investigated for a coarse and fine grids with, respectively, 50% less and 100% more cells with respect to the standard grid. Table 3 tabulates the number of cells employed in the five regions for coarse, standard, and fine grids for the $L/H = 1$ case and Mach number of 25.

In analogous fashion, an examination was made in the y-direction with a coarse and fine grids with, respectively, 50% less and 100% more cells with respect to the standard grid only in the y-direction. In addition, each grid was made up of a non-uniform cell spacing in both directions. Moreover, point clustering is used close to

Table 3 Number of cells in the (x–direction) and [y–direction] investigation for the $L/H = 1$ case.

	Coarse	Standard	Fine
R1	(10×80)	20×80	(40×80)
	[20×40]		[20×160]
R2	(65×110)	130×110	(260×110)
	[130×55]		[130×220]
R3	(10×110)	20×110	(40×110)
	[20×55]		[20×220]
R4	(65×120)	130×120	(260×120)
	[130×60]		[130×240]
R5	(20×40)	40× 40	(80×40)
	[40×20]		[40×80]

solid walls and to the horizontal plane connecting the two corners. The effect (not shown) of changing the cell size in both directions on the heat transfer, pressure and the skin friction coefficients along the gap surfaces was rather insensitive to the range of cell spacing considered, indicating that the standard grid, with a total of 35,300 cells, for the $L/H = 1$ case, is essentially grid independent.

In a second stage of the grid independence investigation, a similar examination was made for the number of molecules. The standard grid for the $L/H = 1$ case corresponds to, on average, a total of 741,200 molecules. Two new cases using the same grid were investigated. These two new cases correspond to 370,600 and 1,482,400 molecules in the entire computational domain. As the three cases presented the same results (not shown) for the heat transfer, pressure and skin friction coefficients along the gap surfaces, hence the standard grid with a total of 741,200 molecules is considered enough for the computation of the flowfield properties. A discussion of the effects of the cell size, number of molecules, and time step variations on the aerodynamic surface quantities for the gaps presented herein is described in detail by Paolicchi [19].

6 Computational Results and Discussion

This section focuses on the calculations of the primary properties obtained from the DSMC results. The primary properties of particular interest in this work are velocity, density, pressure, and temperature. Therefore, the purpose of this section is to discuss differences in these properties due to variations on the gap L/H ratio and on the freestream Mach number.

6.1 Velocity Field

The effect of the freestream Mach number on the tangential velocity profiles for two sections inside the gap is illustrated in Fig. 3 parameterized by the gap L/H ratio. In this set of plots, the tangential velocity u, i.e., the velocity component in the x–direction, is normalized by the freestream velocity U_∞, X'_L represents the distance $(x - L_u - L/2)$ normalized by the gap length L, Y_H stands for the height y normalized by gap depth H. In addition, filled symbols (FS) and empty symbols (ES) correspond, respectively, to the velocity profiles for freestream Mach number of 5 and 25. Results for Mach number of 15 are intermediate, and they will not be shown. Particular attention should be paid to the fact that U_∞ differs from one case to another.

According to Fig. 3, at the bottom surface, Y_H = -1, the tangential velocity ratio is negative. From the bottom to the top of the gap, the velocity ratio u/U_∞ becomes positive at a section Y_H that depends on the L/H ratio. For the $M_\infty = 5$ case, at section X'_L = -0.25, the velocity ratio u/U_∞ changes from negative to positive values at section Y_H of -0.28, -0.15, -0.10, and -0.07 for L/H ratio of 1, 1/2, 1/3, and 1/4, respectively. On the other hand, at $X'_L = 0.25$, u/U_∞ changes from negative to positive values at Y_H of -0.35, -0.18, -0.12, and -0.09 for L/H ratio of 1, 1/2, 1/3, and 1/4, respectively. Therefore, it is firmly established that the thickness of the separated boundary layer decreases with decreasing the L/H ratio, and it slightly increases from section X'_L = -0.25 to $X'_L = 0.25$.

Normal velocity profiles as a function of the streamwise distance X'_L are displayed in Fig. 4

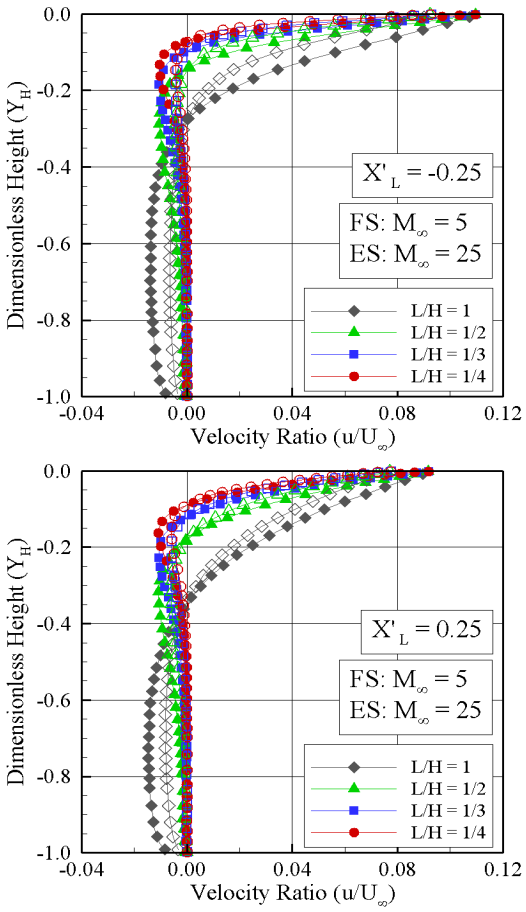

Fig. 3 Tangential velocity (u/U_∞) profiles as a function of the L/H ratio for section X'_L of (a) -0.25 and (b) 0.25 inside the gaps.

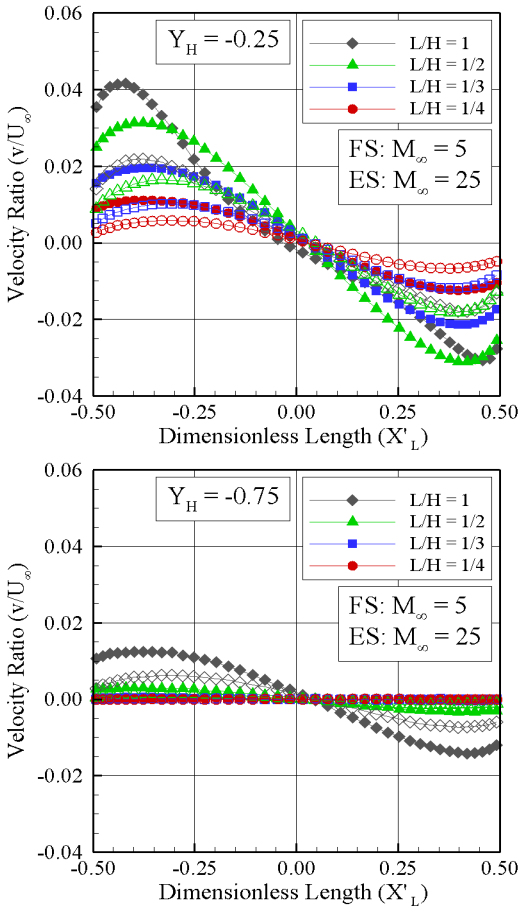

Fig. 4 Normal velocity (v/U_∞) profiles for section Y_H of (a) -0.25 and (b) -0.75 inside the gaps.

parameterized by the gap L/H ratio. In this group of plots, the normal velocity v, i.e., the velocity component in the y–direction, is normalized by the freestream velocity U_∞, Y_H = -0.25 corresponds to the section close to the top of the gap, and Y_H = -0.75 that one close to the bottom. Again, filled symbols (FS) and empty symbols (ES) correspond, respectively, to the velocity profiles for freestream Mach number of 5 and 25. According to these figures, near the gap backward face, $-0.50 < X'_L < -0.25$, the v-velocity component profiles present positive values for the L/H ratio investigated, meaning that the fluid is moving upward. Close to the gap forward face, $0.25 < X'_L < 0.50$, the normal velocity profiles present negative values, pointing out that the flow is moving downward, thus indicating the presence of a region of clockwise circulating flow. Particular attention is paid to the velocity profiles for the $L/H < 1/2$ cases near the bottom of the gaps, i.e., for Y_H = -0.75. It is quite apparent that the velocity component v is zero, indicating that there is no a recirculation region at the vicinity of the gap floor for these cases.

In order to gain some insight into the physics of the flowfield structure, streamline traces inside the gaps are displayed in Figs. 5 and 6 for Mach number of 5 and 25, respectively. In this group of plots, dimensionless height Y stands for the vertical distance y normalized by the freestream mean free path λ_∞.

Looking first at Fig. 5, it is clearly noticed that the flow within the gaps is characterized by the appearance of a recirculation region, as pointed out earlier. For the L/H cases investigated, the streamline pattern shows that the flow is characterized by a primary vortex system. For

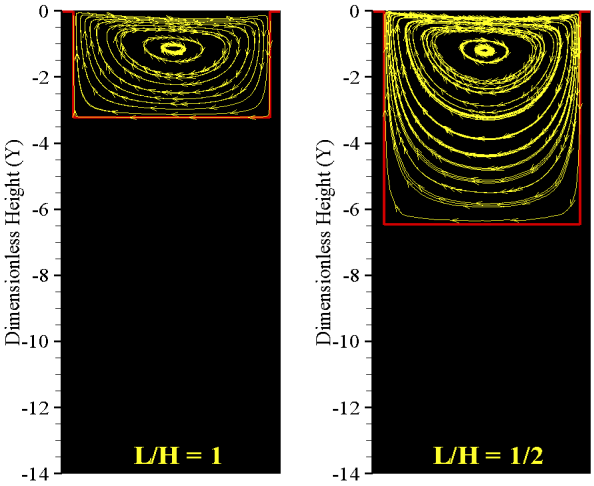

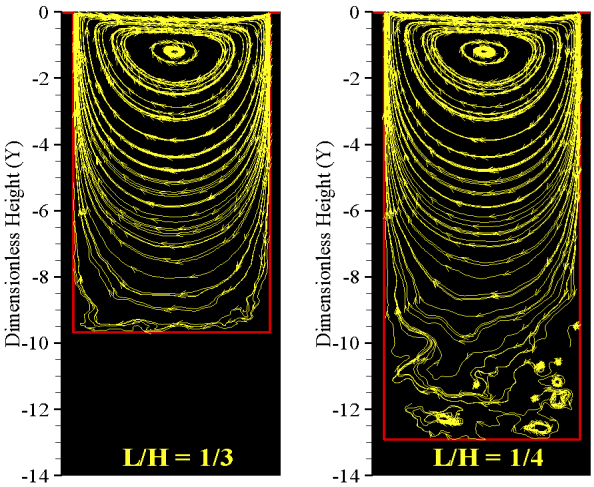

Fig. 5 Distribution of streamline traces inside the gaps for freestream Mach number of 5 and L/H ratio of (a) 1, (b) 1/2, (c) 1/3, and (d) 1/4.

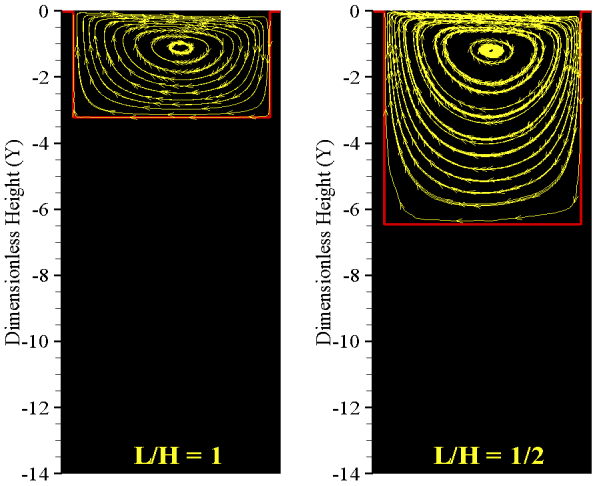

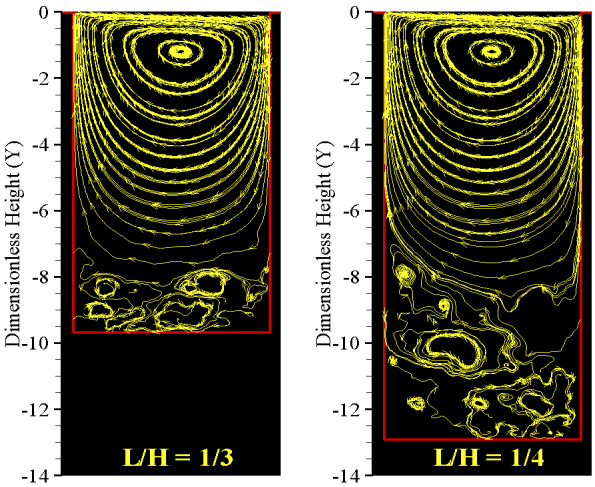

Fig. 6 Distribution of streamline traces inside the gaps for freestream Mach number of 25 and L/H ratio of (a) 1, (b) 1/2, (c) 1/3, and (d) 1/4.

the $L/H \leq 1/3$ cases, it is noteworthy that the recirculating structure fills the entire gaps. Conversely, for the $L/H = 1/4$ case, the recirculating structure does not fill the entire gap. In addition, as expected, the external stream does not reattach the floor of the gap. Moreover, it should be mentioned that the gap flow topology observed herein in a rarefied environment differs from that usually observed in the continuum flow regime. In general, in the continuum flow regime, the gap flow topology [20] is defined by the development of a column of counter-rotating vortices within the gap caused by the main stream flow, where the number of vortices is approximately given by the amount of H/L. In addition, alternating hot spots are developed in the gap when the vortices directionally align and impinge on the gap sidewall.

Turning next to Fig. 6, streamline traces for the $M_\infty = 25$ case, it is observed that the flow topology is similar to that one shown for the $M_\infty = 5$ case in the sense that it is also characterized by only one vortex core. By visual inspection, it is noticed the recirculation regions for gaps with L/H ratio of 1/3 and 1/4 are smaller than those for the $M_\infty = 5$ case. Moreover, the recirculating structure does not fill the entire gaps,

in contrast to that for $M_\infty = 5$ case.

6.2 Density Field

The impact of compressibility in the density profiles is demonstrated in Fig. 7 parameterized by the L/H ratio. In this group of plots, density ratio stands for the density ρ normalized by the freestream density ρ_∞, filled symbols (FS) and empty symbols (ES) correspond, respectively, to the section X'_L of -0.25 and 0.25. In addition, due to the large range of variation for the ratio ρ/ρ_∞, the scale in the x–axis differs from one plot to another.

Based on these plots, it is clearly seen that density ratio shows significant changes as the freestream Mach number increases from 5 to 25. For the $M_\infty = 5$ case, it is seen that density ρ is lower than the freestream density ρ_∞. Furthermore, density ratio close to the gap backward face, section X'_L = -0.25, is lower than that close to the forward face, section X'_L = 0.25. The reason for that is because the flow experiences an expansion on the corner of the backward face, i.e., at the surface S1/surface S2 junction, and a compression on the forward-face corner. In contrast, for the $M_\infty = 25$ case, density ρ is larger than the freestream density ρ_∞. It is noticed that, inside the gaps, density ratio presents lower values on the top of the gaps, i.e., at section Y_H = 0.0, and higher values at the gap bottom surfaces, i.e., Y_H = -1.0. Moreover, it is apparent that the density ratio tends to a constant value at the bottom of the gap with decreasing the L/H ratio.

6.3 Pressure Field

The influence of the freestream Mach number on pressure profiles inside the gaps is depicted in Figs. 8. In this set of plots, again filled symbols (FS) and empty symbols (ES) correspond, respectively, to the section X'_L of -0.25 and 0.25. In addition, due to the large range of variation for the ratio p/p_∞, the scale in the x–axis differs from one plot to another. According to these plots, it is very encouraging to observe that, in general, the pressure ratio inside the gaps decreases from the top to the bottom of the gaps for the freestream Mach number investigated. Also,

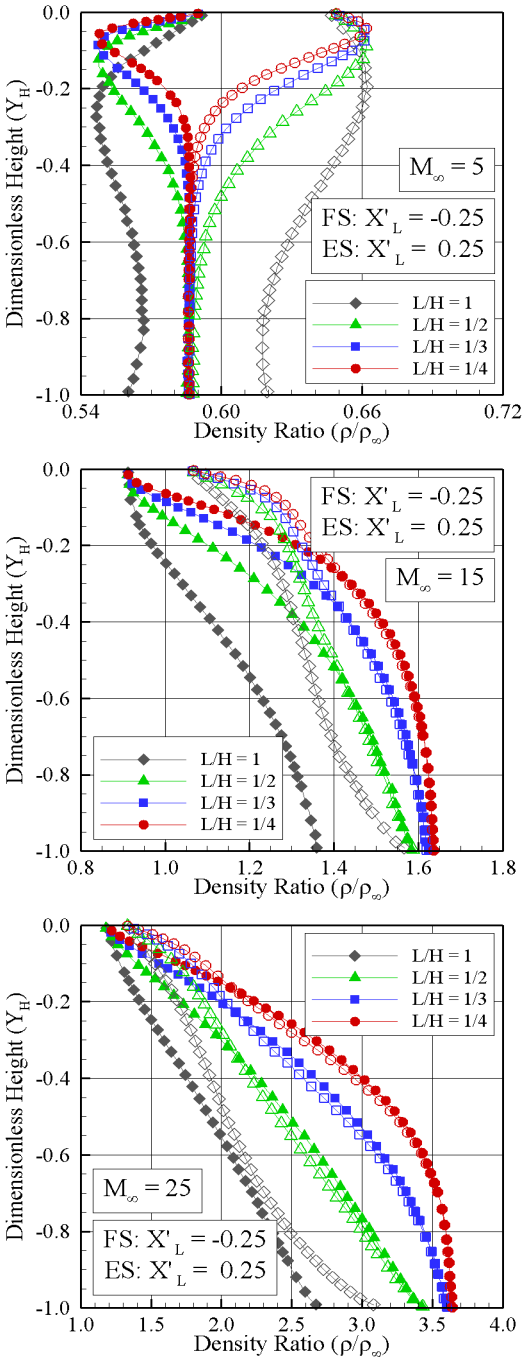

Fig. 7 Density ratio (ρ/ρ_∞) profiles for two sections inside the gap as a function of the L/H ratio for M_∞ of (a) 5, (b) 15, and (c) 25.

similar to the density ratio, the pressure ratio tends to a constant value at the bottom of the gaps with decreasing the L/H ratio. Moreover, as indeed is clear from these plots, at the bottom of the gaps, the pressure p is one order of magnitude larger than the freestream pressure p_∞ for

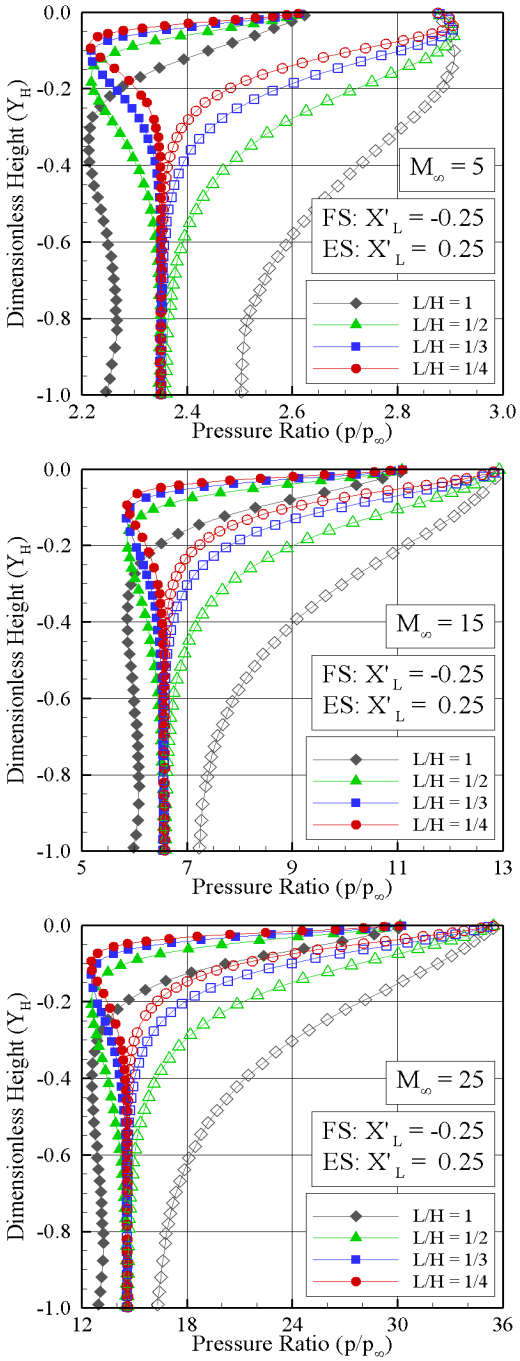

Fig. 8 Pressure ratio (p/p_∞) profiles for two sections inside the gap as a function of the L/H ratio for M_∞ of (a) 5, (b) 15, and (c) 25.

the $M_\infty = 25$.

6.4 Kinetic Temperature Field

Compressibility effects on the kinetic temperature distribution at the centerline of the gaps are displayed in Fig. 9. In this group of plots, temperature ratio stands for the translational temperature T_T, rotational temperature T_R, or vibrational temperature T_V normalized by the freestream temperature T_∞. Also, filled (FS) and empty (ES) symbols correspond to temperature distributions for gap L/H ratio of 1 and 1/4, respectively. Temperature profiles for the other cases are intermediate and they are not shown.

According to these plots, it is clearly noticed that thermodynamic non-equilibrium occurs inside the gaps, as shown by the lack of equilibrium of the translational and internal kinetic temperatures. Thermal non-equilibrium occurs when the temperatures associated with translational, rotational, and vibrational modes of a polyatomic gas are different from one to each other. In general, the temperature ratio decreases from the top to the bottom of the gaps. At the vicinity of the gap bottom surface, it is seen that the flow reaches the thermal equilibrium for the $L/H = 1/4$ case, once the internal temperatures are equal to the translational temperature. Close to the bottom surface, the temperature corresponds to the wall temperature T_w ($\approx 4T_\infty$). It is important to recall that, the density increased at the vicinity of the gap bottom surface by increasing the freestream Mach number as well as by decreasing the gap L/H ratio, as was illustrated in Fig. 7. Consequently, the local mean free path decreased and the mean collision frequency increased and, therefore, the flow reached the thermal equilibrium.

It should be mentioned in this context that, in a non-equilibrium gas, an overall kinetic temperature is defined [13] as the weighted mean of the translational and internal temperature by the following expression,

$$T_O = \frac{\zeta_T T_T + \zeta_R T_R + \zeta_V T_V}{\zeta_T + \zeta_R + \zeta_V} \qquad (1)$$

were ζ is the degree of freedom and subscript T, R and V stand for translation, rotation and vibration, respectively.

The overall kinetic temperature T_O is equivalent to the thermodynamic temperature only in thermal equilibrium conditions. As a matter of fact, it should be noticed that the ideal gas equation of state does not apply to this temperature in a non-equilibrium situation. In this fashion,

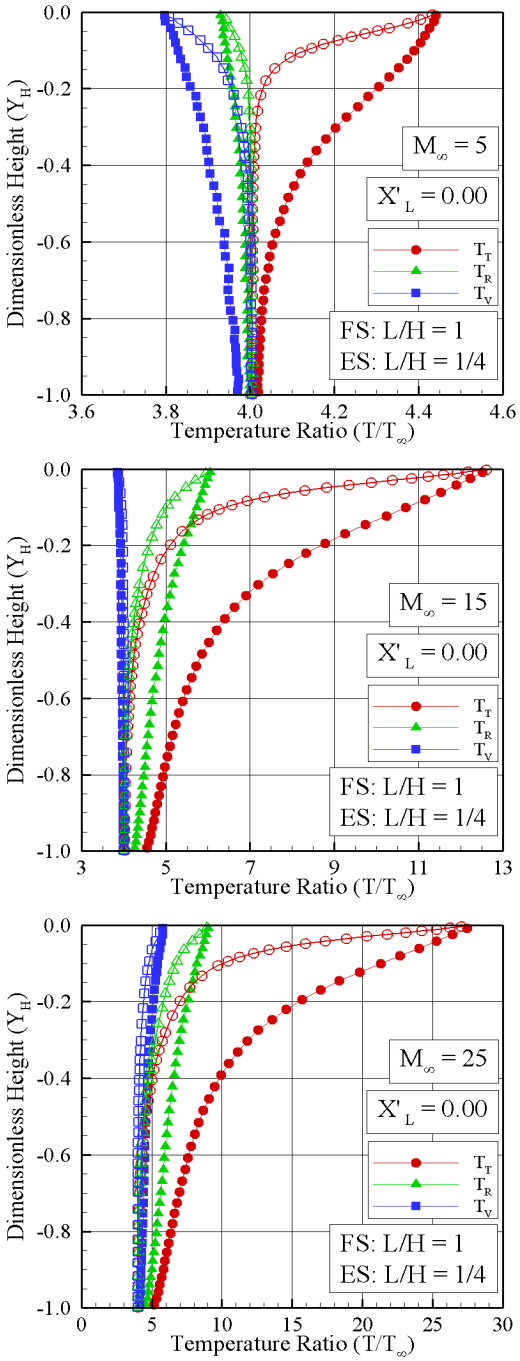

Fig. 9 Kinetic temperature ratio (T/T_∞) profiles at the center of the gap for L/H ratio of 1 and 1/4 and M_∞ of (a) 5, (b) 15, and (c) 25.

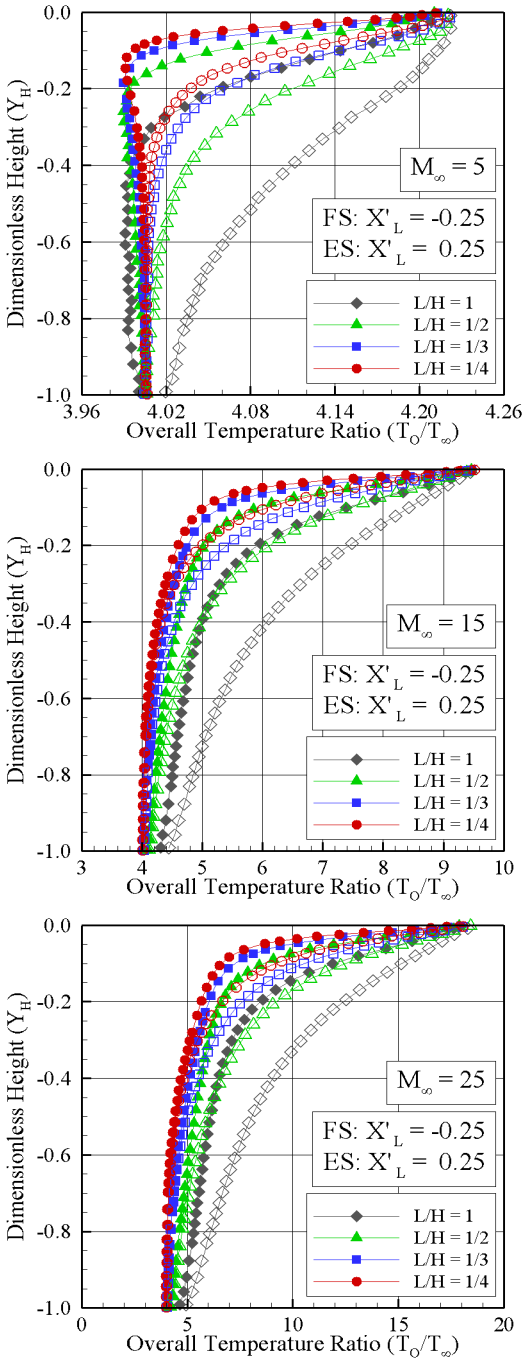

Fig. 10 Overall kinetic temperature ratio (T_O/T_∞) profiles for two sections inside the gap as a function of the L/H ratio for M_∞ of (a) 5, (b) 15, and (c) 25.

Fig. 10 demonstrates the influence of compressibility on the overall kinetic temperature profiles as a function of the gap L/H ratio. Once again, in this set of plots, filled symbols (FS) and empty symbols (ES) correspond to sections X'_L of -0.25 and 0.25, respectively.

7 Concluding Remarks

In an effort toward modeling the compressibility impact on the flowfield structure of a family of gaps in a rarefied hypersonic flow, a detailed nu-

merical study has been developed by using the Direct Simulation Monte Carlo (DSMC) method. The simulations provided information concerning the nature of the primary properties within the gaps. Effects of the freestream Mach number and of the length-to-depth (L/H) ratio on velocity, density, pressure and temperature were investigated for a representative range of parameters. The freestream Mach number ranged from 5 to 25, and the L/H ratio ranged from 1 to 1/4, which corresponded Knudsen numbers in the transition flow regime.

The analysis showed the flowfield structure inside the gaps in the transition flow regime differed from that found in the continuum flow regime, for the conditions investigated in the present account. It was found the flowfield structure is a function of the L/H ratio. It was found only one vortex core for the L/H ratio investigated. It was also found the primary properties behavior inside the gaps for Mach number of 5 differed markedly from those for Mach number of 15 and 25. In contrast, the behavior of the properties for Mach number of 15 was similar to that for Mach number of 25.

References

[1] Dunavant J. C. and Throchmorton D. A. Aerodynamic heat transfer to RSI tile surfaces and gap intersections. *Journal of Spacecraft and Rockets*, Vol. 11, No. 6, pp. 437–440, 1974.

[2] Scott C. D. and Maraia R. J. Gap heating with pressure gradients. *14th AIAA Thermophysics Conference*, Orlando, FL, USA, AIAA Paper 79–1043, 1979.

[3] Bertin J. J. and Goodrich, W. D. Aerodynamic heating for gaps in laminar and trasitional boundary layers. *18th AIAA Aerospace Sciences Meeting and Exhibit*, Pasadena, CA, USA, AIAA Paper 80–0287,1980.

[4] Pitts W. C. and Murbach, M. S. Flight measurements of tile gap heating on the space shuttle. *AIAA/ASME 3rd Joint Thermophysics, Fluids, Plasma and Heat Transfer Conference*, St. Louis, MO, USA, AIAA Paper 82–0840, 1982.

[5] Smith D. M., Petley D. N., Edwards C. L. W. and Patten A. B. An investigation of gap heating due to stepped tiles in zero pressure gradient regions of the shuttle orbiter thermal protection system. *21st AIAA Aerospace Sciences Meeting and Exhibit*, Reno, NV, USA, AIAA Paper 83-0120, 1983.

[6] Petley D. H., Smith D. M., Edwards C. L. W., Carlson A. B. and Hamilton II H. H. Surface step induced gap heating in the shuttle thermal protection system. *Journal of Spacecraft and Rockets*, Vol. 11, No. 2, pp. 156–161, 1984.

[7] Higdon J. J. L. Stokes flow in arbitrary two-dimensional domains: shear flow over ridges and cavities. *Journal of Fluid Mechanics*, Vol. 159, pp. 195–226, 1985.

[8] Charbonnier J. and Boerrigter H. Contribution to the study of gap induced boundary layer transition in hypersonic flow. *AIAA/DGLR 5th International Aerospace Planes and Hypersonics Technologies Conference*, Munich, Germany, AIAA Paper 93–5111, 1993.

[9] Hinderks M., Radespiel R., and Gülhan A. Simulation of hypersonic gap flow with consideration of fluid structure interaction. *34th AIAA Fluid Dynamics Conference and Exhibit*, Portland, OR, USA, AIAA Paper 2004–2238, 2004.

[10] Traineau J. C., Thivet F., Gulhan A., Cosson E., Smith A., and Marraffa L. Synthesis of the gap heating analysis of the hyflex flight. *Proceedings of the Fifth European Symposium on Aerothermodynamics for Space Vehicles*, Cologne, Germany, 2004.

[11] Hinderks M., and Radespiel R. Investigation of hypersonic gap flow of a reentry nosecap with consideration of fluid structure interaction. *44th AIAA Aerospace Sciences Meeting and Exhibit*, Reno, NV, USA, AIAA Paper 2006-0188, 2006.

[12] Paolicchi L. T. L. C. and Santos W. F. N. Length-to-depth ratio effects on aerodynamic surface quantities of a rarefied hypersonic gap flow. In: *44th AIAA Thermophysics Conference*, San Diego, CA, USA, AIAA Paper 2013–2789, 2013.

[13] Bird G. A. *Molecular gas dynamics and the direct simulation of gas flows*, 1st edition, Oxford University Press, 1994.

[14] Bird G. A. Monte Carlo simulation in an engineering context. *Progress in Astronautics and Aeronautics: Rarefied gas Dynamics*, AIAA New York, Vol. 74, pp. 239–255, 1981.

[15] Bird G. A. Perception of numerical method in rarefied gasdynamics. *Rarefied Gas Dynamics: Theoretical and Computational Techniques*, Progress in Astronautics and Aeronautics, AIAA, New York, Vol. 118, pp. 374–395, 1989.

[16] Borgnakke C. and Larsen P. S. Statistical collision model for Monte Carlo simulation of polyatomic gas mixture. *Journal of Computational Physics*, vol. 18, pp. 405–420, 1975.

[17] Boyd I. D. Analysis of rotational nonequilibrium in standing shock waves of nitrogen. *AIAA Journal*, Vol. 28, pp. 1997–1999, 1998.

[18] Bird G. A. A Comparison of collision energy-based and temperature-based procedures in DSMC. *26th International Symposium on Rarefied Gas Dynamics*, American Institute of Physics, pp. 245–250, 2009.

[19] Paolicchi L. T. L. C. Computational analysis of gap effects on the surface of reentry apace vehicles. MS Thesis, National Institute for Space Research (INPE), Combustion and Propulsion Laboratory, 2010.

[20] Everhart J. L., Alter S. J., Merski N. R., Wood W. A., and Prabhu R. K. Pressure gradient effects on hypersonic cavity flow heating. *44th AIAA Aerospace Sciences Meeting and Exhibit*, Reno, Nevada, USA, AIAA Paper 2006–0185, 2006.

Copyright Statement